bioRxiv preprint doi: https://doi.org/10.1101/2021.05.24.445519; this version posted May 25, 2021. The copyright holder for this preprint (which was not certified by peer review) is the author/funder, who has granted bioRxiv a license to display the preprint in perpetuity. It is made available under aCC-BY-NC-ND 4.0 International license.

Cryptic genetic variations of alanine:glyoxylate aminotransferase shape its fitness and dynamics

Mirco Dindo[1], Stefano Pascarelli[1], Davide Chiasserini[2], Silvia Grottelli[2], Claudio Costantini[2], Gen-Ichiro Uechi[1], Giorgio Giardina[3]*, Paola Laurino[1]*, Barbara Cellini[2]*

[1]Okinawa Institute of Science and Technology Graduate University, 1919-1 Tancha, Onna-son, Kunigami, Okinawa 904-0495, Japan.

[2]Department of Medicine and Surgery, University of Perugia, P.le L. Severi 1, 06132 Perugia, Italy

[3]Department of Biochemical Sciences "A. Rossi Fanelli", Sapienza University of Rome, Italy.

*these authors contributed equally to this work. Correspondence to: Giorgio Giardina (giorgio.giardina@uniroma1.it); Paola Laurino (paola.laurino@oist.jp); Barbara Cellini (barbara.cellini@unipg.it)

bioRxiv preprint doi: https://doi.org/10.1101/2021.05.24.445519; this version posted May 25, 2021. The copyright holder for this preprint (which was not certified by peer review) is the author/funder, who has granted bioRxiv a license to display the preprint in perpetuity. It is made available under aCC-BY-NC-ND 4.0 International license.

Abstract

Genetic variations expand the conformational landscape of proteins and may underlie cryptic functions able to influence protein adaptability under unfavorable conditions. Cryptic functions usually associate with regions of increased frustration or even intrinsically disordered, whose role as drivers of innovation is increasingly being recognized. Hence, the balance between protein stability and "controlled" disorder translates in the dichotomy between conservation and innovability, and should be regarded as the more comprehensive measure of protein fitness. In this context, understanding how genetic variations affect protein fitness is not trivial, since cryptic functions behind frustrated regions are not easily detectable. Herein, we used as model the pyridoxal 5'-phosphate (PLP)-dependent enzyme alanine:glyoxylate aminotransferase (AGT), which is present as a common major allelic form (AGT-Ma) and a minor polymorphic form (AGT-Mi) expressed in 20% of Caucasian population and considered a lower limit of AGT fitness. By solving the structure of AGT-Mi, we could show that three distinct regions, that are structured in AGT-Ma, are disordered in AGT-Mi. Molecular dynamics shows that AGT-Mi samples more flexible conformations than AGT-Ma, supporting a plasticity effect propagated to all the structure. In-depth biochemical characterisation of mutants from a small library of variants encompassing the three regions reproduces the fitness window between AGT-Ma and AGT-Mi. Cellular studies highlight the consequences of this plasticity at functional level and suggest the existence of cryptic functions likely related to protein-protein interactions. These results establish that naturally-occurring genetic variations tip the balance between protein stability and frustration to encode cryptic functions that expand the potential innovability of the protein.

bioRxiv preprint doi: https://doi.org/10.1101/2021.05.24.445519; this version posted May 25, 2021. The copyright holder for this preprint (which was not certified by peer review) is the author/funder, who has granted bioRxiv a license to display the preprint in perpetuity. It is made available under aCC-BY-NC-ND 4.0 International license.

INTRODUCTION

Proteins can exhibit underlaying functions that cannot be phenotypically observed, but represent a genetic potential that might emerge as favorable under rapid selection conditions, a phenomenon called "cryptic" genetic variation (1). The importance of cryptic genetic variations is becoming increasingly evident as they contribute to protein evolvability, innovability, and adaptability to cellular stresses, but also because they can increase our understanding of the emergence of complex diseases as well as of the role of modifier factors in the phenotypic expression of rare mutations. In this regard, cryptic alleles represent a trade-off between an advantageous adaptation when an unusual condition becomes common, and the generation of polymorphic traits that increase disease susceptibility (2, 3). Is it possible to unravel the structural basis of this trade-off?

Cryptic genetic variations can have subtle effects on a protein structure that are difficult to identify. Often they widthen the protein conformational sampling, by increasing the degree of disorder. An extreme consequence of a wide conformational sampling is that of protein regions that are conformationally frustrated and thus explore an excess of flexibility at the edge of disorder (fuzzyness), or simply don't have a defined structure, i.e. intrinsically disordered regions (IDRs) (4). This structural plasticity can be beneficial for a protein since it can mediate the interaction with multiple binding partners.(5, 6). At the same time, however, increasing frustration and disorder negatively affects protein stability, which in turn can decrease protein fitness in a specific intracellular environment -herein we refer to protein fitness as the ensemble of properties contribuiting to the function(s) of a protein, such as protein's stability and activity. However, how evolution balances cryptic genetic variations hidden behind the conformational plasticity of frustrated regions or IDRs and how they can have a relapse on protein fitness remains poorly understood.

Liver peroxisomal alanine:glyoxylate aminotransferase 1 (AGT1) is a dimeric pyridoxal-5' phosphate (PLP)-dependent enzyme that transaminates L-alanine and glyoxylate to pyruvate and glycine, respectively; a reaction crucial for glyoxylate detoxification (7). Numerous naturally-occurring variants of AGT1 are known, some of which are associated with the life-threatening condition named Primary Hyperoxaluria Type I (PH1) characterized by the progressive accumulation of calcium oxalate stones first in the urinary tract, and then at systemic level (8, 9). Besides pathogenic forms, it is of note that 20% of the Caucasian population express a polymorphic form of AGT1 called minor allele (AGT-Mi) differing from the more common major allele (AGT-Ma) for the P11L and I340M substitutions (10). AGT-Mi is not pathogenic *per se*, but can influence the effects of other mutations in a form of genetic epistasis (11, 12). Indeed, AGT-Ma and AGT-Mi have been proposed as two limit forms for

bioRxiv preprint doi: https://doi.org/10.1101/2021.05.24.445519; this version posted May 25, 2021. The copyright holder for this preprint (which was not certified by peer review) is the author/funder, who has granted bioRxiv a license to display the preprint in perpetuity. It is made available under aCC-BY-NC-ND 4.0 International license.

AGT1 thermodynamic and kinetic stability, placing AGT-Mi at the edge of misfolding, so that any further destabilizing mutation leads to a decrease in protein fitness resulting in aggregation and premature degradation (13, 14). The fact that AGT-Mi it is still retained in the human genome and did not go through purging selection during evolution strongly suggests that it must constitute a potential source of protein innovability. Thus, AGT1 represents an ideal model to understand how nature compromises on structure stability to ensure potential innovability. On the other hand, the tight dependency of AGT1 fitness on the cellular environment makes it an ideal protein model to understand the interplay between protein fitness and cellular functional constraints. Nevertheless, since no structural information is available for AGT-Mi, the evolutionary rationale behind the co-esistance of AGT-Mi and AGT-Ma in human cells represents an unmet challenge.

In this work, we have performed a systematic study of AGT1 showing that AGT-Ma retains a certain degree of conformational plasticity that is increased to a limit represented by AGT-Mi, ultimately underlays genetic cryptic variations. Structural analyses reveal that AGT-Mi comprises three disordered regions, whose dynamics is the results of an enhanced conformational flexibility of the N-terminal arm that propagates through all the structure due to the presence of conformational frustration. A mainly “anti-consensus” library of AGT-Ma in these three regions reveals the biochemical and biophysical aspects related to the transition from the fitness of AGT-Ma to the lowest limit of fitness represented by AGT-Mi. Finally, studies in eukariotyc cells demonstrate that an altered conformational plasticity affects intracellular stability and interaction with binding partners, suggesting that cryptic genetic variants can shape the cellular interactome.

bioRxiv preprint doi: https://doi.org/10.1101/2021.05.24.445519; this version posted May 25, 2021. The copyright holder for this preprint (which was not certified by peer review) is the author/funder, who has granted bioRxiv a license to display the preprint in perpetuity. It is made available under aCC-BY-NC-ND 4.0 International license.

RESULTS

The crystal structure of AGT-Mi unveils three unexpected disordered regions

The structure of AGT-Mi was solved by X-ray crystallography at 2.2 Å resolution (**Fig. 1**). The I340M mutation was clearly observed as a sharp positive electron density peak corresponding to the sulphur atom position (**Fig. S1A**). On the other hand, no electron density was observed for the N-terminal residues (residues 1 to 10 :MASHKLLVTP) (**Fig. S1B**), indicating that the P11L mutation results in a loss of defined structure in this region. In the AGT1 dimer the N-terminal arm is involved in an important interaction between the monomers, and mutations altering its conformation are known to affect protein thermodynamic and kinetic stability (14-16). Thus, our data provide a definitive proof for many biochemical and *in silico* studies performed in the last decade, which have suggested that the lower stability of AGT-Mi was linked to a disordered N-terminus (16-20). Surprisingly, we found the presence of another

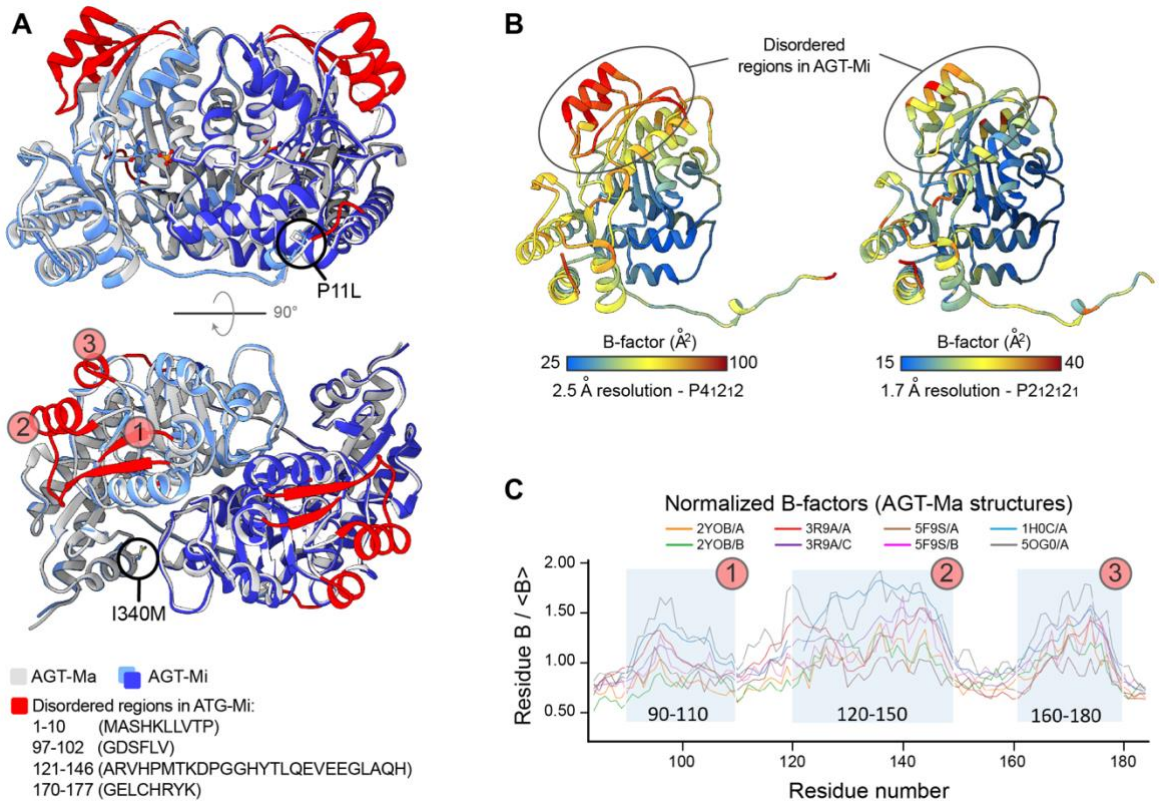

Figure 1 Structure of AGT-Mi. A) Cartoon representation of the structure of AGT-Mi superposed on AGT-Ma (PDB: 5F9S). The two subunits of AGT-Mi are shown in dark and light blue while for AGT-Ma are shown in white and dark grey. The regions that were not included in the model of AGT-Mi, due to disorder, are coloured in red in the structure of ATG-Ma. With the exception of the N-terminus, the other disordered regions are numbered from 1 to 3 and correspond to residue stretches 97-102, 121-146 and 170-177, respectively. **B**) Two AGT-Ma structures solved at different resolution and in different space groups are coloured according to temperature factor (B-factors) values (PDBs: 5OG0 and 5F9S on the left and right side, respectively). Both structures show high B-factors in the region that are disordered in ATG-Mi. **C**) Analysis of normalized B-factors over the range of all available AGT-Ma structures in different space groups. High B-factors values correspond to the disordered regions (1, 2 and 3) in AGT-Mi. These regions are not involved in crystal contacts, therefore the observed disorder is not a consequence of crystal packing. The B-factor of the structure 2YOB is the lowest, suggesting a destabilizing effect of the P11L mutation balanced by a stabilizing effect of the I340M mutation.

bioRxiv preprint doi: https://doi.org/10.1101/2021.05.24.445519; this version posted May 25, 2021. The copyright holder for this preprint (which was not certified by peer review) is the author/funder, who has granted bioRxiv a license to display the preprint in perpetuity. It is made available under aCC-BY-NC-ND 4.0 International license.

disordered region in AGT-Mi: an undefined electron density was observed for residues 97-102 (GDSFLV), 121-146 (ARVHPMTKDGGHYTLQEVEEGLAQH) and 170-177 (GELCHRYK), which were not included in the final model **(Fig. S1 C, D)**. In AGT-Ma these regions form two α-helices and two β-strands at the periphery of the large domain (the structural unit binding PLP) (**Fig. 1A**) that tend to display a higher mobility in all the structures solved to date, with temperature factors (B-factors) that appear systematically higher than the mean values of each structure (**Fig. 1 B, C**). The polymorphic mutations typical of the minor allelic form of AGT not only induce a conformational change at the mutation site, but also in a structurally frustrated region of AGT1, resulting in an increased disorder. Thus, AGT1-Mi is characterized by the presence of IDRs. This observation is extremely important since IDRs in globular proteins usually consist of the terminal regions or represent interdomain linkers (21). In addition, the shift between order and disorder is usually influenced by ligand or partner binding rather than by naturally-occurring polymorphic mutations (6).

Testing the plasticity of IDRs by Molecular Dynamics allow to rationalize the effects of AGT-Mi mutations

Next, we inverstigated the AGT1 conformational sampling by molecular dynamics (MD) simulations. We aimed at detecting any difference between the conformers sampled by the PLP-bound AGT-Ma and AGT-Mi. The stable AGT-Ma conformation (PDB:5F9S) was used as a model and as a starting point for the single- and double-mutant models. The single-mutant models were obtained by individually mutating P11L or I340M, while the double-mutant model was obtained by mutating both positions together, to achieve the AGT-Mi model (more details in the Methods). After an equilibration step, the models were run for 200 ns in five repeats (**Fig. 2A**).

The simulations confirmed that the regions identified as IDRs in AGT-Mi by crystallography also fluctuate in AGT-Ma (**Fig 2A**), as suggested by B-factor analysis (**Fig. 1B-C**), indicating that these regions are prone to disorder (frustrated) in AGT-Ma too. However, in AGT-Mi the N-terminus (residues 6-18) and the helix 48-64 quickly sample a range of alternative conformations due to an increase of the fluctuations in these regions that is not observed in the AGT-Ma simulations (**Fig. 2A**). Notably, this helix is in close contact with both the very dynamic C-terminus domain and several regions involved in PLP binding (**Fig 2A**). From the simulation results, it appears that the multiple conformations adopted by AGT-Mi results from backbone dynamics initiated by an increased fluctuation of the helix 48-64 and the N-terminus, which propagates through the C-terminus and the active site to the IDRs (**Fig. S2A**). Analysis of protein local frustration, nicely correlates with this hypothesis, showing that in AGT-Ma regions of high conformational frustration cluster along the same route indicated by maximal

bioRxiv preprint doi: https://doi.org/10.1101/2021.05.24.445519; this version posted May 25, 2021. The copyright holder for this preprint (which was not certified by peer review) is the author/funder, who has granted bioRxiv a license to display the preprint in perpetuity. It is made available under aCC-BY-NC-ND 4.0 International license.

fluctuation and connecting the N- and C-terminus dynamics (**Fig. 2B** and **movie S1**). Interestingly, Free Energy Surface (FES) analysis confirmed that AGT-Mi uniquely explores a set of conformations at high RMSD and gyration radius where the C-terminus helices and parts of the IDRs are notably displaced (**Fig 2C**). In the IDRs, this apparently small detachment of the two helices may indeed weaken the hydrophobic interactions that stabilize the structured state leading to a disordered conformation. Furthermore, MD simulations of the single mutant P11L showed enhanced fluctuations of the N-terminus tail (**Fig. S2B**), and a higher occupancy of the conformations at high radius of gyration (**Fig. S2C**). This result highlights the structural determinants of the stabilizing effect of the I340M mutation that we observed in the MD simulation of this single mutant and also in previous studies (22). In fact, Ile340 is placed at the interface between helix 48-64 and the C-terminus and its substitution with a longer hydrophobic side chain partially reduces the dynamics of these regions (**Fig S2D**).

bioRxiv preprint doi: https://doi.org/10.1101/2021.05.24.445519; this version posted May 25, 2021. The copyright holder for this preprint (which was not certified by peer review) is the author/funder, who has granted bioRxiv a license to display the preprint in perpetuity. It is made available under aCC-BY-NC-ND 4.0 International license.

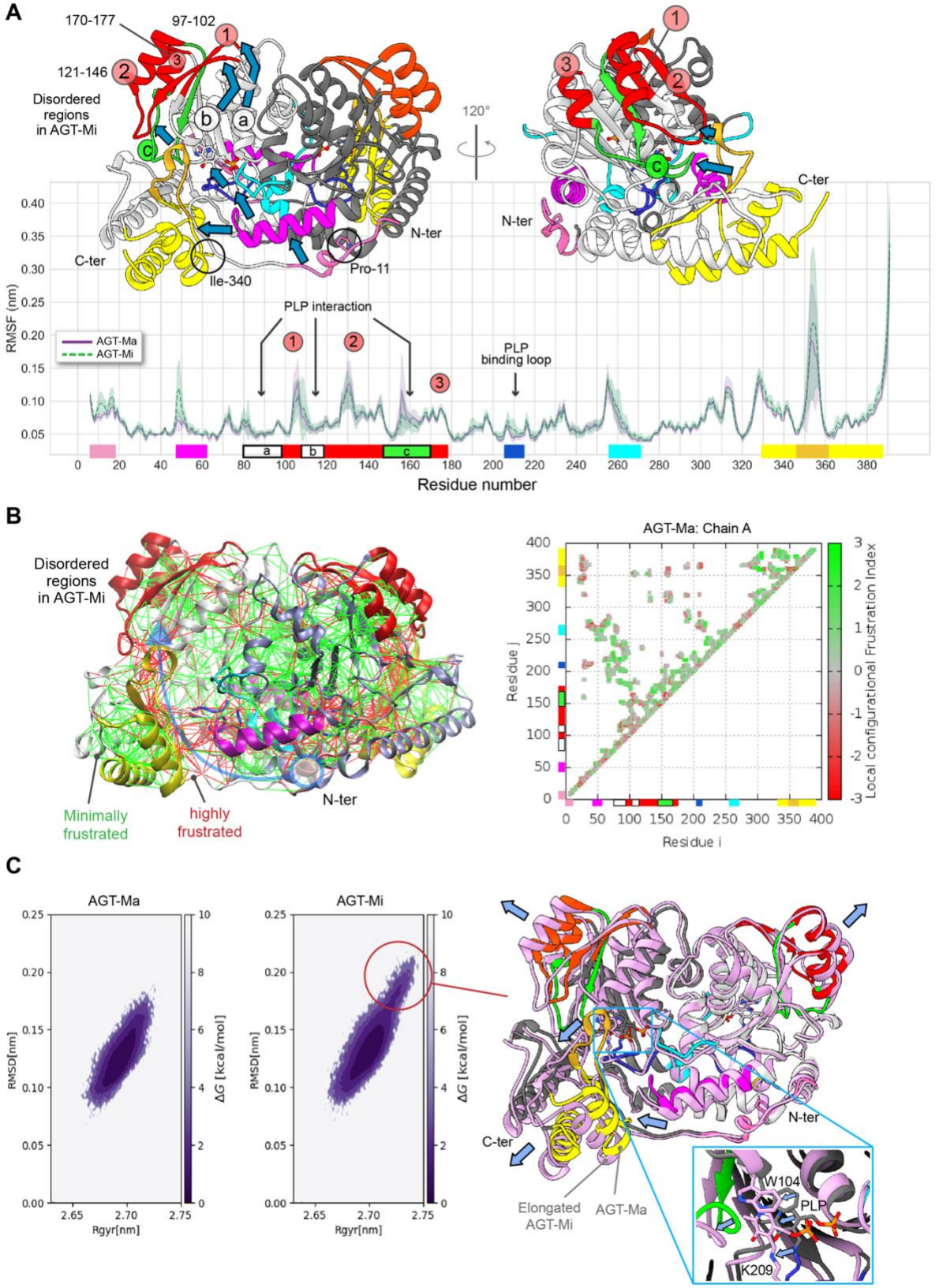

Figure 2: Molecular dynamics simulations. A) Plot of the root mean square fluctuation (RMSF) as a function of residue number: AGT-Ma (purple) and AGT-Mi (green). The different regions are mapped over the AGT-Ma structures in different colours, that are also reported on the plot axis to indicate both the extension and the colour of each region. The increased mobility of the N-terminus (in *pink*) and especially of the residues 48-64 (in *magenta*) of AGT-Mi may cause a domino effect that is propagated through the C-terminus (in *yellow*) and three structural regions (indicated with *a*, *b* and *c*) that are directly

bioRxiv preprint doi: https://doi.org/10.1101/2021.05.24.445519; this version posted May 25, 2021. The copyright holder for this preprint (which was not certified by peer review) is the author/funder, who has granted bioRxiv a license to display the preprint in perpetuity. It is made available under aCC-BY-NC-ND 4.0 International license.

interacting with PLP and with the disordered regions 1, 2 and 3(in *red*). Details on the MD method are reported in Table S2. **B**) AGT-Ma conformational frustration. Green and red connections indicate couples of minimal and maximal frustrated residues, respectively. The configurational frustration index evaluates how the energetic contribution to protein stability of a the interaction between residues *i* and *j* compares to different possible local environment. The interaction is considered frustrated when other conformations with higher stabilization energy are possible (23). Areas of high frustration are localized at the interface of the highly fluctuating regions, connecting the N-terminous to the disordered regions in ATG-Mi (blue arrow). The same colouring of panel A is used to highlight the different portions of AGT both in the structure than in the correlation plot. **C**) Free Energy Surface (FES) of the five combined simulations for AGT-Ma and AGT-Mi. The FES was generated in a similar fashion as in Strodel et al. (24) and using RMSD and gyration radius as the two coordinate systems. On the right, a representative structure of the AGT-Mi in the highlighted region of panel B (with high RMSD and high gyration) is shown in pink, superposed with the structure of AGT-Ma (5f9s) that is depicted with the same coloring pattern of panel A. The loss of secondary structure and displacement (blue arrows) is evident in parts of the disordered regions and in the C-terminus domain. The displacement also affects the cofactor position (inset).

To test the role of the order/disorder transition in a cellular environent, we rationally introduced four mutations - L101A, H146A, L172A, and C173A – that should enhance the plasticity of the IDRs by reducing the number of favourable interactions between the side chains of these regions. As shown in **Fig. S3**, all substitutions in the first and third region (residues 97-102 and 170-177, respectively) do not significantly change AGT1 specific activity and protein level, while the H146A mutation of the second region leads to a significant reduction of soluble protein and active enzyme levels, a finding suggesting that its role could be more pronounced. Overall, by combining the structural, molecular dynamics and cellular data, we highlighted the presence of a structural hotspot that appears as an order-disorder conformational switch for AGT1 in the native state. These results place AGT-Ma and AGT-Mi at the boundaries of an unexpected conformational landscape that is dominated by the equilibrium between order and disorder of the IDRs, with the major allele sampling, on average, ordered conformations and the minor allele *living* on the edge of frustration and disorder.

A library of the disordered regions of AGT hints to the advantage of a structural instability

To gain insights into the role of the IDRs from the evolutionary perspective, we generated a library of AGT-Ma variants in the three regions (residues 97-102; 121-146; 170-177) that showed to be disordered in the AGT-Mi structure. The design of the library was based on two main principles. First, we identified all the positions where the residue conservation is below 80% among the alignment (**Table S3**). Then we identified “anticonsensus” mutations, namely those causing the change of a residue with another one present in nature in the same position but showing a lower abundance (**Fig. 3A**). This choice has been dictated by the need to mimic a subtle destabilization typical of cryptic genetic variations, while avoiding big conformational

bioRxiv preprint doi: https://doi.org/10.1101/2021.05.24.445519; this version posted May 25, 2021. The copyright holder for this preprint (which was not certified by peer review) is the author/funder, who has granted bioRxiv a license to display the preprint in perpetuity. It is made available under aCC-BY-NC-ND 4.0 International license.

changes and keeping intact the AGT1 overall structure. However, positions 127 and 177 are the only ones in which the human sequence does not show a consensus residue. For these two residues, we decided to include also mutations to the residue most represented in other species, with the aim of exploring the possibility of achieving a more stable and active structure at the expenses of the above detected structural plasticity or flexibility.

Second, we used a semi-rational approach, i.e. a strategy based on the random combination of rationally-chosen mutations (see Material and Methods section Cloning and Library construction). As a result, we obtained a small library (48 variants) bearing single, double and triple mutations. Although the library was focused on a region distant from the catalytic site (> 12 Å, **Fig. 3B**), its importance for the overall AGT1 stability allowed the reconstruction of the putative functional intermediates within and beyond the fitness window defined by AGT-Ma and AGT-Mi (**Fig. 3C** and **Fig. S4)**. 21% of the mutants showed specific activity below AGT-Mi, 48% between AGT-Mi and -Ma and 31% above AGT-Ma. The wide range of activity sampled by this library demonstrates the importance of these three regions on the overall structure and gives further information on the effect of the frustration on AGT1. Nonetheless, the effects of these mutants are subtle, a sign suggestive that cryptic variations can shape the order/disorder equlibrium maintained in AGT-Ma.

To explain the fitness outcomes of the mutations introduced on the surface of the disordered regions, we chose two variants with specific activity between AGT-Mi and Ma (S99A, K177Q) and four with specific activity above the one of AGT-Ma (P125Q, T127A, Q145R, E138A/K177Q) for further characterization in the purified form. Upon confirming by CD studies that none of the introduced substitutions caused gross structural changes in AGT1 (**Fig. S5A**), we determined both the melting temperature (**Fig. 3D**) and the kinetic parameters for the transamination reaction, to get insights on possible alterations of global stability and intrinsic functional activity, respectively. The functional characterization of the purified selected variants revealed no significant changes in the kinetic parameters as reported in **Table 1** and **Fig. S6**. In fact, these three regions are distant from the catalytic site (> 12 Å), and the mutations do not directly influence the microenvironment of the cofactor, as shown by the visible bands of the CD spectra of the corresponding variants (**Fig. S5B**). As further confirmation to this observation, also the tertiary structure of the mutants (**Fig. S5B**) is identical to that of AGT-Ma. More interestingly, none of the mutations interfere with the turnover number of the enzyme, thus indicating that the observed changes in specific activity in the bacterial lysate (**Fig. 3C**) can be mainly ascribed to a structural alteration that reduces folding efficiency, possibly implying that the disordered surfaces represent a critical region for the overall AGT1 fitness in a cellular environment.

bioRxiv preprint doi: https://doi.org/10.1101/2021.05.24.445519; this version posted May 25, 2021. The copyright holder for this preprint (which was not certified by peer review) is the author/funder, who has granted bioRxiv a license to display the preprint in perpetuity. It is made available under aCC-BY-NC-ND 4.0 International license.

The analysis of the melting curves of the single variants confirms the reduced thermostability of AGT-Mi with respect to AGT-Ma. The stability of AGT-Ma is not affected or sligthly improved by the T127A, Q145R and K177Q mutations, but is reduced by the S99A and P125Q substitutions to values between that of the two polymorphic forms. Notably, the denaturation

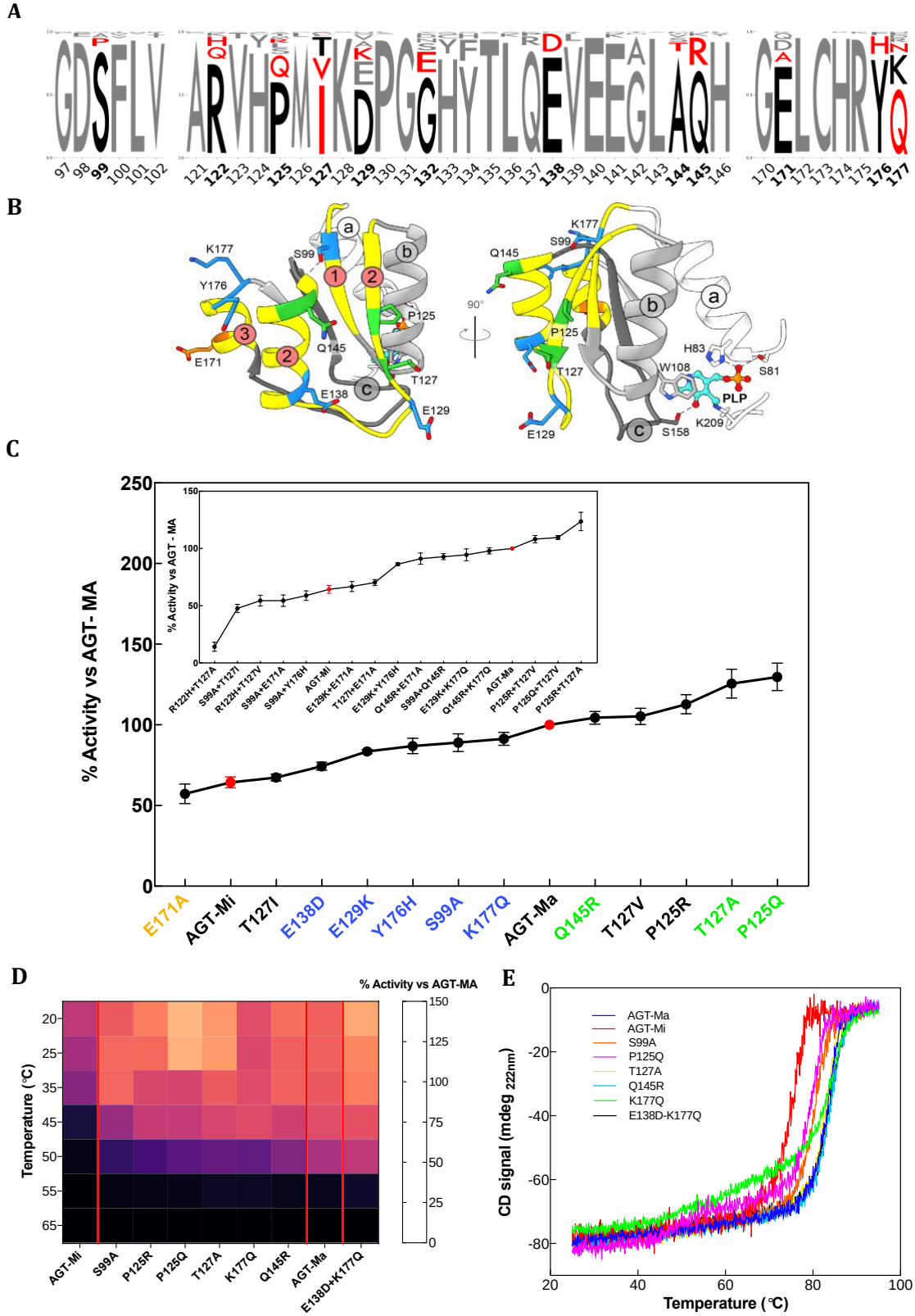

bioRxiv preprint doi: https://doi.org/10.1101/2021.05.24.445519; this version posted May 25, 2021. The copyright holder for this preprint (which was not certified by peer review) is the author/funder, who has granted bioRxiv a license to display the preprint in perpetuity. It is made available under aCC-BY-NC-ND 4.0 International license.

Figure 3 Library construction and mutants biochemical and biophysical characterisation. A) Consensus logo of the three disordered regions studied here. XX The sequences (110-130) from the non-redundant database were collected by blast search and aligned using MUSCLE algorithm on JalviewXX. The logo was generated using Logomaker (https://logomaker.readthedocs.io/en/latest/). In bold black numbers, the positions that were mutated. In black, the aminoacids of the human AGT1 sequence, while in red, the aminoacids considered for the library. **B**) The mutated residues are plotted over the AGT-Ma structures in different colours. In orange the one with activity below AGT-Mi, in blue the ones with activity between AGT-Mi and AGT-Ma, and in green the ones above AGT-Ma. **C**) Residual activity of the indicated variants as compared to AGT-Ma. **D**) Heat map of residual activity of selected mutants obtained after incubating the lysate at different temperatures for 10 minutes. Mutants color code follows that of panel C. **E**) Thermal stability curves of the selected variants represented in panel D. Color code follows panel C.

curves of the P125Q and K177Q variants show the loss of cooperativity on the unfolding of the two domains of AGT1, in line with molecular dynamics results indicating that IDRs on the large domain influence the conformation of the small C-terminal domain where Ile340 is located (26). The latter effect on the single K177Q variant is abolished in the E138/K177Q variant, in agreement with the improved fitness of the double variant upon *E.coli* expression (**Fig. 3C**). Overall, all the mutants included in this library are functionally active, meaning that mutations of the IDRs do not have substantial negative effects on the AGT1 structure. The finding that all the detected changes in stability and activity are subtle suggests that naturally occurring mutations can be easily tolerated while maintaining a fine fitness balance of the protein.

Table S3. Kinetic parameters of AGT-Ma, AGT-Mi and the mutants chosen from the AGT library. Experimental details are given in the Material and Methods.

Enzyme	Substrate	Cosubstrate	k_{cat} (s^{-1})	K_M (mM)	k_{cat}/K_M ($s^{-1}mM^{-1}$)
AGT-Ma[A]	L-alanine	Glyoxylate	45 ± 2	31 ± 4	1.4 ± 0.2
	Glyoxylate	L-alanine	45 ± 3	0.23 ± 0.05	196 ± 44
AGT-Mi[B]	L-alanine	Glyoxylate	33 ± 5	28 ± 2	1.2 ± 0.2
	Glyoxylate	L-alanine	37 ± 1	0.22 ± 0.01	168 ± 8
S99A	L-alanine	Glyoxylate	36 ± 2	29 ± 4	1.2 ± 0.18
	Glyoxylate	L-alanine	34 ± 3	0.31 ± 0.05	109 ± 20
P125Q	L-alanine	Glyoxylate	43 ± 5	55 ± 8	0.78 ± 0.14
	Glyoxylate	L-alanine	35 ± 2	0.22 ± 0.03	159 ± 22
T127A	L-alanine	Glyoxylate	42 ± 3	33 ± 4	1.27 ± 0.17
	Glyoxylate	L-alanine	34 ± 4	0.16 ± 0.03	212 ± 44
Q145R	L-alanine	Glyoxylate	47 ± 4	41 ± 5	1.15 ± 0.17
	Glyoxylate	L-alanine	38 ± 4	0.21 ± 0.04	181 ± 32
K177Q	L-alanine	Glyoxylate	37 ± 3	35 ± 5	1.05 ± 0.17
	Glyoxylate	L-alanine	36 ± 4	0.27 ± 0.06	133 ± 33

bioRxiv preprint doi: https://doi.org/10.1101/2021.05.24.445519; this version posted May 25, 2021. The copyright holder for this preprint (which was not certified by peer review) is the author/funder, who has granted bioRxiv a license to display the preprint in perpetuity. It is made available under aCC-BY-NC-ND 4.0 International license.

E138D/K177Q	L-alanine	Glyoxylate	44 ± 4	53 ± 7	0.83 ± 0.13
	Glyoxylate	L-alanine	39 ± 3	0.27 ± 0.04	145 ± 24

Expression of IDRs variants in a cellular system highlights their role for AGT1 fitness and interactions

To investigate the consequences of the structural frustration of the AGT fitness in the mammalian cellular environment, selected variants with single or double mutations in the putative disordered regions were expressed in HEK293 cells and analysed for specific activity and protein levels (**Fig. 4**).

As expected, cells expressing AGT-Mi displayed a slightly lower specific activity and protein levels as compared to AGT-Ma. The S99A mutation in IDR 1 reduced AGT1 specific activity and protein levels below AGT-Ma. These data are in line with the observation that, while the S99A variant shows intermediate properties between AGT-Ma and AGT-Mi when present alone, all double and triple variants containing the S99A mutation display a fitness lower than AGT-Mi. Some differences between the bacterial and mammalian environment can be observed on variants belonging to the second disordered region. P125Q, T127A and Q145R variants show specific activity values higher than AGT-Ma in the bacterial environment. However, in analogy with the data obtained on the mutation of His146 (**Fig. S3**), the presence of these mutations strongly impairs the specific activity and relative expression of AGT1 in mammalian cells. Indeed, the P125Q variant shows a fitness comparable to AGT-Mi while a lower fitness is observed in the presence of T127A and Q145R mutations. Since Pro125, Thr127 and Gln145 do not affect the kinetic properties of AGT or its intrinsic thermodynamic stability, these results clearly indicate that specific interactions occurring in the mammalian environment could be responsible for the observed changes. It can be suggested that the conformational change caused by the mutation of Thr127 and Gln145 could favour the interaction with components of the quality control network typical of eukariotyc cells (25). Finally, the mutations in the third disordered region are expected to slightly affect protein fitness with L172A and C173A displaying a specific activity similar, if not higher, compared to AGT-Ma (**Fig. S3**). However, the K177Q and E138D/K177Q variants showed specific activity and proteins levels lower than AGT-Ma and similar to those of AGT-Mi, in line with the observed changes of melting temperature caused by the Lys177 mutation.

bioRxiv preprint doi: https://doi.org/10.1101/2021.05.24.445519; this version posted May 25, 2021. The copyright holder for this preprint (which was not certified by peer review) is the author/funder, who has granted bioRxiv a license to display the preprint in perpetuity. It is made available under aCC-BY-NC-ND 4.0 International license.

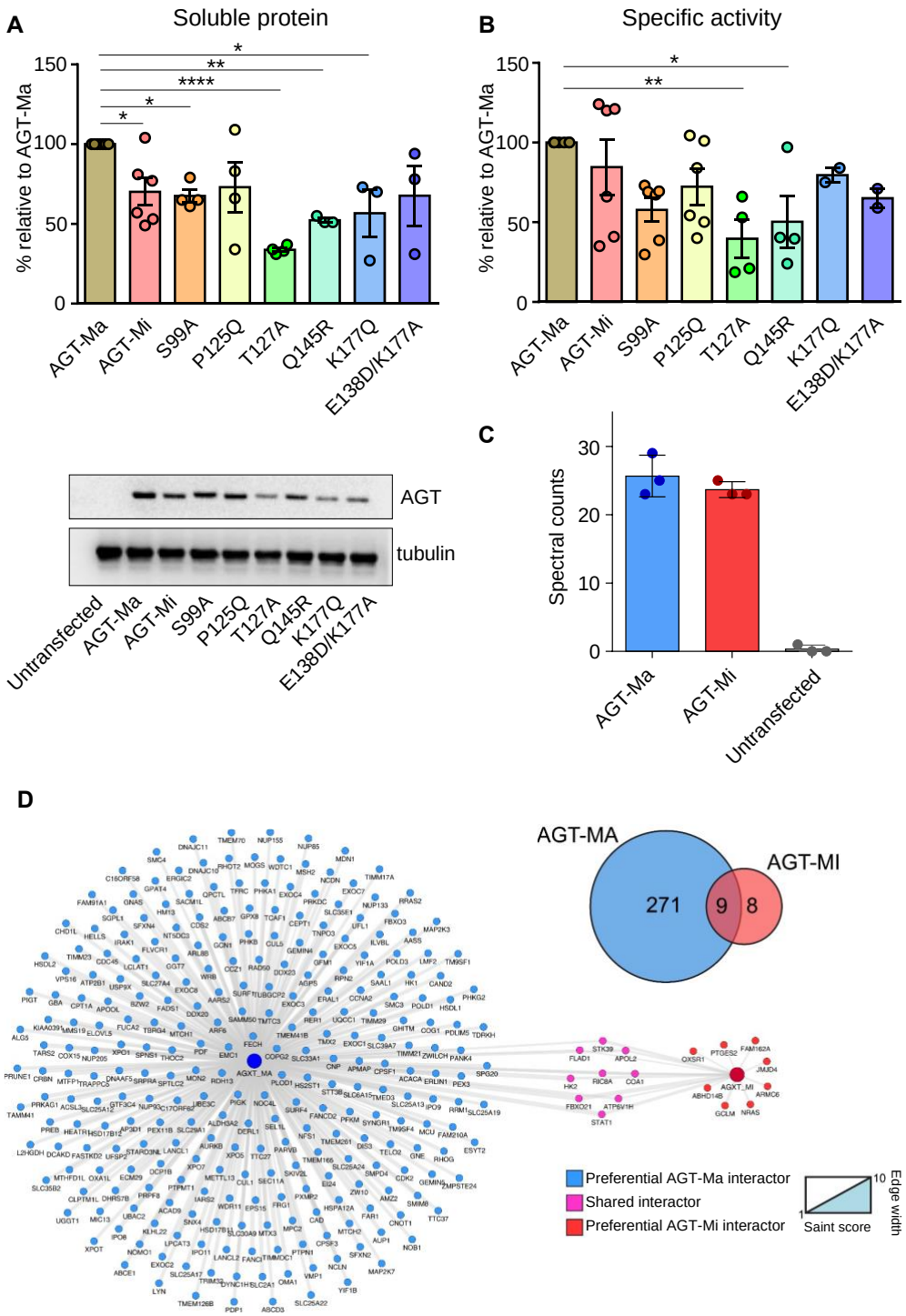

Fig. 4: Expression, specific activity and interactors of AGT-Ma, AGT-Mi, and selected variants in human cells. A) and B) Human Embrionic kidney (HEK) 293 cells expressing the indicated species were harvested and lysed. In panel A, transaminase activity was detected by incubating 90 µg of soluble lysate with 0.5 M L-alanine, 10 mM glyoxylate, and 200 µM PLP at 25 °C in 100 mM KP, pH 7.4. In panel B, soluble protein levels were quantified by western-blot. 15 µg of soluble lysate of each sample were subjected to SDS-PAGE, immunoblotted with anti-AGT from rabbit (1:6000), and detected by chemiluminescence. The histogram is representative of immunoblot band volume (as mean ± SEM of at least three independent experiments). C-D) Interactome of AGT-Ma and AGT-Mi. Panel C shows that AGT1 protein levels were enriched in AGT-Ma and AGT-Mi transfected samples after immunoprecipitation using a a pan anti-AGT1 antibody. Control samples (Ctrl) showed undetectable levels of AGT; Panel D shows Venn diagram of significant interactions compared to controls between AGT-Ma and AGT-Mi and the interaction network of AGT-Ma and AGT-Mi isoforms. Nodes are representative of proteins described with gene name, edges' width is proportional to SAINT score vs control samples.

bioRxiv preprint doi: https://doi.org/10.1101/2021.05.24.445519; this version posted May 25, 2021. The copyright holder for this preprint (which was not certified by peer review) is the author/funder, who has granted bioRxiv a license to display the preprint in perpetuity. It is made available under aCC-BY-NC-ND 4.0 International license.

Overall, these data allow to conclude that introducing mutations in residues belonging to IDRs can affect protein fitness in a cellular environment, suggesting that the potential involvement of IDRs in AGT1 interactions with binding partners.

To analyse the interactome of the two AGT isoforms we used co-immunoprecipitation coupled with quantitative mass spectrometry (IP-MS). HEK293 cells transfected with AGT-Ma and AGT-Mi showed a similar number of identified proteins compared to controls not expressing AGT (~3000, data not shown). Label-free quantification of AGT showed a significant enrichment of both AGT-Ma and AGT-Mi isoforms compared to control samples in which AGT was basically not detectable (**Fig. 4C**). SAINT analysis of the interactions of AGT-Ma and AGT-Mi indicated a marked difference in the preferential interactome of the two isoforms (**TableS6**). According to our filtering criteria versus control IPs, AGT-Ma showed 280 significant interactions while AGT-Mi only 17 (**Fig. 4D**). Overlap analysis of the interactions between the two isoforms showed also a minimal overlap with 9 proteins interacting with both AGT-Ma and AGT-Mi.

DISCUSSION

The main finding of this work is that AGT1 is endowed with a high conformational plasticity (fuzziness), due to the presence of structurally frustrated regions. AGT-Ma and AGT-Mi structurally differ for the degree of disorder of three peripheral regions, and represent the limits of the functional-fitness window of AGT. The evolutionary conservation of frustrated regions that renders an enzyme less tolerant to mutations seems counterintuitive, but AGT1 is a paradigmatic example of how unstable regions are preserved by evolution as they underlay cryptic functions that might serve to function in protein-protein interactions. In the subtle trade-off between a stable structure, favouring the catalytic activity, and a more flexible one, that allows multiple interactions, evolution optimizes both functions by keeping the degree of disorder within a strict fitness window (**Fig. 5**).

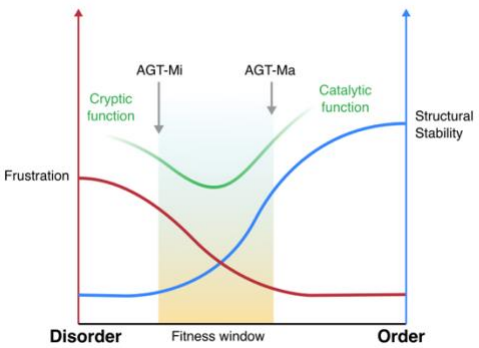

Fig. 5. Scheme representing the fitness window of AGT1 as resulting from the order/disorder switch that balances structural stability (blue curve) and frustration (red curve).

bioRxiv preprint doi: https://doi.org/10.1101/2021.05.24.445519; this version posted May 25, 2021. The copyright holder for this preprint (which was not certified by peer review) is the author/funder, who has granted bioRxiv a license to display the preprint in perpetuity. It is made available under aCC-BY-NC-ND 4.0 International license.

We immediately recognise the AGT1 polymorphism as a powerful model system to explore how point mutations may affect protein fitness. We explored this aspect by constructing a small-scale "anti-consensus" library and found that it not only sampled the entire fitness range from AGT-Mi to AGT-Ma, but also identified variants with higher activity and/or stability than AGT-Ma. Although it is not possible to rationalize the effect of each mutation, we noticed as expected that changes affecting less conserved residues seem to give rise to more deleterious effects, while those affecting more conserved residues seem to be generally advantageous. However, none of the mutations dramatically decrease or increase the protein fitness.

It is therefore likely that the conformational plasticity of AGT due to the presence of IDRs may have been conserved by evolution for their ability to balance between the two opposite forces of structural stability and innovability. This would agree with recent studies showing that proteins showing IDRs play a role during the first stages of speciation due to their tolerability to mutations ((26). Therefore, the evolutionary advantage goes beyond the catalytic efficiency to encompass the stability/function/interactions in a cellular enviroment. From the structural perspective, perturbation of the frustrated regions with naturally occurring substitutions results in subtle thermostability and activity changes of the purified proteins or in a bacterial cell background, whereas when the mutants are investigated in a eukariotic cellular context a new role of these IDRs is uncovered. The frustated regions therefore play a crucial role for AGT stability in the cell with AGT-Ma maximising both the interactions and the activity and AGT-Mi beenig at the edge of misfolding. If the protein is forced outside this window either ways (i.e. to an IDR situation or to a too stable structure) it loses one of the functions.

Our data on the behaviour of selected single variants of the library expressed in Hek293 cells confirm this hypothesis, by showing that mutations affecting the frustated regions that render AGT-Ma more stable and active (i.e. T127A and Q145R), reduce the intracellular stability of AGT in terms of both protein levels and specific activity. On the other hand, mutations that shift the equilibrium of the native conformers towards a disordered state may induce aggregation or degradation upon sensing by the quality control systems (25). In this regard, previous data have shown that the two polymorphic P11L and I340M typical of the minor allele oppositely affect the propensity of native AGT to aggregation mediated by electrostatic forces (22). Our data not only confirm and structurally explain these observations, but also allow to re-interpret the effects of two PH1-associated mutations that occur in region 2 (D129H and E141D) and were predicted to cause the AGT deficit by changing the electrostatic potential surface (22). It is likely that these mutations modify the degree of disorder of region 2 with consequences on the intracellular stability of the protein.

Indeed, our proteomic data clearly show that the interactome of the two polymorphic forms of AGT is different in both quantitative and qualitative terms. Although the detailed analysis of

bioRxiv preprint doi: https://doi.org/10.1101/2021.05.24.445519; this version posted May 25, 2021. The copyright holder for this preprint (which was not certified by peer review) is the author/funder, who has granted bioRxiv a license to display the preprint in perpetuity. It is made available under aCC-BY-NC-ND 4.0 International license.

the interactors at functional level goes beyond the scope of this work, we observed that AGT1 seems to retain the possibility to interact with partners involved in mitochondrial protein import and/or assembly (**Table S6**). It can be speculated that this property represents a vestigial of the mitochondrial localization of AGT1 that has been lost as a consequence of an adaptive shift in AGT targeting, under the evolutive pressure of a diet change from mainly carnivorous to omnivorous and herbivorous (27). AGT-Mi minimizes but still retains few interactions. Then why has a minor allele polymorphism been retained during evolution? A purging selection during evolution could have easily left only one copy of AGT1, since we were able to sample many AGT1 variants with a stability and activity comparable or even better then AGT-Ma with just a small library, however two polyphormic forms of AGT1 are present in human population. This cannot be the outcome of chance and must rather be the result of a necessity, maybe to preserve a vestigial of innovation.

In summary, our work has broader implications into our view of proteins that display a flat-bottom folding funnel, because the native state is not unique but fluctuates among different conformers, the conformational landscape of such proteins can be greatly influenced by either environmental changes or naturally-occurring mutations. Following this idea, and especially in the case of metabolic enzymes, the fitness of the whole cell depends on a pool of different conformers with distinct functions; it depends on the necessity to balance catalysis with networking. From an evolutionaty point of view, the fate of a protein would then not only depend on the generation of partly-folded intermediates, but also from the equilibrium between “functional” or “potentially noxious” native conformers, which in turn depends on surface residues whose importance has been underestimated in classical biochemical and protein folding studies. In this regard, a growing number of reports point to natural polymorphisms, including those related to IDRs, as key contributors to human diseases (28, 29), and that single amino acid changes common in human population more likely affect binding interfaces with other proteins or nucleic acids (30).

The AGT case is a very clear example of evolutionary “risk-management”: a certain degree of instability and disorder, although it may lead to misfunction, is retained and “controlled” in order to achieve additional or cryptic functions (multitasking).

Materials and Methods

Reagents-Pyridoxal phosphate (PLP), L-alanine, sodium glyoxylate, rabbit muscle L-lactic dehydrogenase (LDH), β-Nicotinamide adenine dinucleotide reduced form (NADH) and isopropyl-β-D-thiogalactoside (IPTG) were purchased from Sigma-Aldrich. Protease Inhibitor Cocktails organic solvents were purchased from Nacalai tesque. All other chemicals unless otherwise noted, were from Sigma-Aldrich, Nacalai tesque or Wako.

bioRxiv preprint doi: https://doi.org/10.1101/2021.05.24.445519; this version posted May 25, 2021. The copyright holder for this preprint (which was not certified by peer review) is the author/funder, who has granted bioRxiv a license to display the preprint in perpetuity. It is made available under aCC-BY-NC-ND 4.0 International license.

Crystallography of AGT-Mi and structure determination-Single crystals of AGT-Mi were obtained by vapor diffusion methods (sitting drop) mixing 0.4 µl of a 37 µM protein solution (buffer: 0.1 M potassium phosphate pH=7.4) with 0.4 µl of the A9 solution of the Morpheus screen (Molecular Dimension), containing: 30 mM MgCl 2 , 30 mM CaCl 2 , 50 mM sodium 4-(2-hydroxyethyl)-1-piperazineethanesulfonate (HEPES) + 50 mM 3-(N-morpholino)propanesulfonic acid (MOPS) at a final pH 7.5, 40% v/v Ethylene glycol; 20 % w/v PEG 8K. Yellow diamond-shaped crystals of about 100-120 µm grew in 1 week. Crystals were flash frozen without prior addition of cryoprotectant. A complete X-ray diffraction dataset was collected at the Elettra synchrotron in Trieste (IT) at XRD1 beamline. The data were processed with XDS 2 and scaled with Aimless 3–5 initially in $P4_1\ 2_1\ 2$ space group to a final resolution of 2.0 Å. However, the observed intensities were very different from the theorical values suggesting the presence of twinning. Indeed, although a very clear molecular replacement solution was found in $P4_1\ 2_1\ 2$ - using the AGT-Ma structure as search model (pdb: 5F9S6) - and the electron density maps were very clear, the model refined to poor R free and geometry values with respect to the resolution of the data. Therefore, different space groups were evaluated and finally the data were reindexed in $P4_1$ with merohedral twin operator h, -k, -l and an estimated twin fraction of 0.44 (Phenix.xtriage 7) that converged to 0.49 during twin refinement in Refmac5 or Phenix.refine 7–9. Given the almost perfect twin, model building was carried out in Coot 10 using electron density maps calculated ignoring twinning, since twin-refinement may introduce a strong model-bias, and with an extensive and careful use of omit-maps. Twin-refinement was used only in the final refinement cycle. Data collection and refinement statistics are summarized in **Table S1** and the quality of the electron density maps is illustrated in **Fig. S1**. Coordinates and structure factors have been deposited in the protein data bank with pdb code: 7NS7. B-factor analysis of AGT-Ma solved structures was performed in Phenix GUI using structure comparison tool 7 . Figures were rendered using Chimera 11.

Molecular Dynamics of AGT-Mi and AGT-Ma-The dimeric structure of AGT-Ma (PDB ID 5F9S) was used as starting point of MD simulations, and as template for the generation of the mutant structures. The monomeric structure of the mutants was obtained through the Swiss-model web server (31), realigned to the reference structure, and manually added of the PLP atoms. PDB file manipulation was performed using pdb-tools (32). By following the procedure of Gupta *et al.,* a hybrid residue named 'LYP' was created by combining the PLP and the Lysine 209 atoms in the PDB file and manually parametrized in the forcefield using the same values reported in the paper (33). All simulations were performed using GROMACS version 2020.3 (www.gromacs.org) (34) and CHARMM36-mar2019 forcefield (35). The model was solvated in a dodecahedral box using 3 points charge water model (tip3p) (36). After charge,

bioRxiv preprint doi: https://doi.org/10.1101/2021.05.24.445519; this version posted May 25, 2021. The copyright holder for this preprint (which was not certified by peer review) is the author/funder, who has granted bioRxiv a license to display the preprint in perpetuity. It is made available under aCC-BY-NC-ND 4.0 International license.

temperature, and pressure equilibration, each simulation run 200 ns in 2 fs steps (four repeats). A modified Berendsen thermostat was used to maintain the temperature at 310K (37), and a Parrinello-Rahman barostat was used to maintain a pressure of 1 bar (38). A Particle Mesh Ewald (PME) was used for long-range electrostatic interactions (39). More details about the system setup and simulation parameters are provided as Supplementary Information.

Expression and purification of AGT1 and variants-E. coli BL21(DE3) cells were transformed with the constructs encoding AGT-Ma, AGT-Mi and the selected variants of the library. Expression and purification of the proteins were performed as reported (7).

Site directed mutagenesis-Mutants were constructed as described in the Q5 Site-Directed Mutagenesis manual (New England Biolabs). The primers list is reported in **Table S4**.

Frustration analysis-Analysis of protein frustration was performed by uploading the AGT-Ma structure (pdb: 5F9S) (40) to the Frustratometer server (http://frustratometer.qb.fcen.uba.ar/) (23) First a list of interacting residues are computed ($Q_{i,j}$) and the native energy of the structure is calculated according to the AMW energy function (41). Frustration between a given couple of amino acids (i,j) is then calculated by perturbating the protein sequence and calculating the total energy change. The contact is then considered minimally frustrated, neutral or highly frustrated according to how favoreble the interaction is compared to all possible interaction. Conformational frustration was visualized using VMD molecular graphics software (42).

Kinetics Assays-To determine the kinetic parameters for the transamination reaction, the purified proteins (0.1-0.2 µM) were incubated in presence of 100 mM PLP in KP 0.1 M pH 7.4 at 25 °C at increasing alanine concentrations (15 to 500 mM) or glyxylate concentrations (0.07 to 5 mM) and a fixed glyoxylate (10 mM) or alanine (500 mM) concentration. The reaction was quenched by adding TCA 10% (v/v) and pyruvate production was measured using a spectrophotometric assay coupled with LDH following the NADH signal at 340 nm (7). To determine the activity in crude bacterial cell lysates, a Tecan Spark Microplate Reader (Thermo Fischef Scientific) was used and the cells were grown and lysed as described below under the section 'Library Screening'.

To measure the enzymatic activity in HEK293 cellular lysates, 100 µg of lysate were incubated with 0.5 M L-alanine and 10 mM glyoxylate at 25°C for 20-60 min in 100 mM KP buffer, pH 7.4 in the presence of 100 µM PLP. The reactions were stopped by adding TCA 10% (v/v) and pyruvate production was measured using a spectrophotometric assay coupled with lactate dehydrogenase (43).

bioRxiv preprint doi: https://doi.org/10.1101/2021.05.24.445519; this version posted May 25, 2021. The copyright holder for this preprint (which was not certified by peer review) is the author/funder, who has granted bioRxiv a license to display the preprint in perpetuity. It is made available under aCC-BY-NC-ND 4.0 International license.

Circular Dichroism spectroscopy- Circular Dichroism (CD) spectra were obtained using a Jasco J-820 spectropolarimeter with a thermostatically controlled compartment at 25 °C. In the near-UV and visible spectra, protein concentration was 10 μM in a cuvette with a path length of 1 cm. Far-UV measurements were taken at a protein concentration of 0.1 mg/ml using a cuvette with a path length of 0.1 cm. The thermal unfolding of AGT-Ma, AGT-Mi and variants was monitored by following the loss of CD signal at 222 nm at a protein concentration of 5-8 μM with temperature increasing of 0.5 °C/min from 25 to 90 °C. The experiments were performed in KP 0.1 M pH 7.4.

Cloning and library construction-The AGT1 sequence (human) (uniprot: P21549, SPYA_HUMAN) was used for conducting NCBI BLAST searches across the non-redundant database. Database search conditions were filtered for search results with query coverage >80% and sequence identity between 70-90% were considered for the next step. The collected sequences were then subjected to multiple sequence alignment using MUltiple Sequence Comparison by Log-Expectation (MUSCLE). The library was prepared using a modified Combinatorial Assembly PCR protocol. The three different regions of interest (97-102, 121-146 and 170-177) were mutated using single stranded mutagenic degenerated primers (**Table S5**) that anneal each other at their edges. The PCR fragments of the three regions of interest were cloned in the pTrcHis2A plasmid by Megawhop cloning (44) and mixed between them to obtain random combination of double and triple mutants. The library was then transformed in BL21 (DE3) E. coli strain and more than 2000 clones were screened.

Library screening-Library has been cloned into pTrcHis-2A, transformed into *E. coli* BL21 (DE3) and plated on ampicillin LB-agar plates. Colonies were picked into deep 96-well plates and grown overnight at 30 °C in 500 μL LB per well supplemented with 50 μg/mL ampicillin. Wells containing fresh LB/ampicillin (2 mL) were inoculated with 100 μL of this preculture, and protein expression was induced adding 0.1 mM IPTG at 25 °C for 16-18 hours. Cells were pelleted by centrifugation and the supernatant removed. Cell lysis was performed by freezing for 60 minutes at −80 °C, and resuspending in 200 μL of sodium phosphate buffer pH 7.4 and supplemented with 100 μg/mL lysozyme, proteinase inhibitor cocktail (Nacalai tesque) and 25 U/mL benzonase (Merck). The mixture has been incubated for 30 min at room temperature. Cell debris was pelleted by centrifugation and 20–100 μL of clarified lysate were removed and tested for AGT1 activity. The activity was tested in presence of 10 μM PLP and saturating concentration of substrate and cosubstrate (10 mM glyoxylate and 500 mM l-alanine) in 200 μL of KP 0.1 M pH 7.4. Some variants were picked and regrown in triplicate, and the rates re-measured and the average values determined. Plasmid DNA was isolated, and variants were

bioRxiv preprint doi: https://doi.org/10.1101/2021.05.24.445519; this version posted May 25, 2021. The copyright holder for this preprint (which was not certified by peer review) is the author/funder, who has granted bioRxiv a license to display the preprint in perpetuity. It is made available under aCC-BY-NC-ND 4.0 International license.

sequenced. The plasmids were retransformed, and the resulting chosen mutants were used to inoculate new cultures for protein purification.

Cell culture, transfection, and lysis-Human Embryonic Kidney cells (HEK293 cells) were cultured in Dulbecco's modified Eagle's medium (DMEM) supplemented with fetal bovine serum (FBS) (10%, v/v), penicillin (100 units/ml) and streptomycin (100 µg/ml) at 37 °C in a 5% CO_2 humidified environment. To test the effects of different AGT1 single amino-acid substitutions on the expression level and enzymatic activity of AGT, cells were seeded in Petri dishes at the density of $2.1x10^4/cm^2$ in DMEM. After 24h of subculture, cells were transfected with different AGT1 constructs using Lipofectamine LTX and PLUS Reagent (Invitrogen) according to the manufacturer's instructions. After 24 h, cells were harvested and used for Western Blotting analyses and enzymatic activity assays. For Co-IP experiments, stable clones of HEK293 cells expressing AGT-Ma or AGT-Mi were generated by selecting transfected cells with 1 mg/ml G418 in the culture medium for three weeks.
For enzymatic activity assays and western-blot analyses cell pellets were lysed by freeze/thawing (five cycles) in PBS (Phosphate Buffer Saline), pH 7.2 supplemented with 100 mM PLP and protease inhibitor cocktail (CompleteMini, Roche). The whole cell extract was separated by centrifugation (12,900 x *g,* 10 min, 4 °C) to obtain the soluble fraction. The pellets were then resuspended in an equal volume of denaturing gel loading buffer to obtain the insoluble fraction. Protein concentration in the soluble fraction was measured using the Bradford protein assay.

Western-Blot and Co-immunoprecipitation-Ten µg of soluble and insoluble cell lysate were loaded on 10% SDS-PAGE, transferred on a nitrocellulose membrane and immunoblotted with anti AGT antibody (1:10.000) in 2.5% milk w/v in TTBS (50mM Tris-HCl, pH 7.5, 150 mM NaCl, 0.1% Tween 20) overnight at 4°C. After three washes in TBST, the membrane was incubated with peroxidase-conjugated antirabbit immunoglobulin G (IgG) (1:10.000) in 5% milk in TTBS for 1 hour at room temperature. Immunocomplexes were visualized by an enhanced chemiluminescence kit (ECL, Pierce Biotechnology, Rockford, IL). An antibody against human tubulin was used as internal loading control.
Co-immunoprecipitation was performed using the Pierce™ Co-Immunoprecipitation Kit according to manufacturer's instructions (Thermo-Scientific). Briefly, cell pellets were lysed in the IP Lyses/Wash Buffer included in the kit, supplemented with protease inhibitor cocktail (CompleteMini, Roche) and phosphatase inhibitors (Sigma-Aldrich). The whole cell extract was separated by centrifugation (12,900 x *g,* 10 min, 4 °C) to obtain the soluble fraction. Two mg of soluble cell lysate from untransfected (negative control) or transfected cells (AGT-Ma and AGT-Mi) were incubated with 10 mg of molyclonal anti-AGT primary antibody, immobilized

bioRxiv preprint doi: https://doi.org/10.1101/2021.05.24.445519; this version posted May 25, 2021. The copyright holder for this preprint (which was not certified by peer review) is the author/funder, who has granted bioRxiv a license to display the preprint in perpetuity. It is made available under aCC-BY-NC-ND 4.0 International license.

on column according to the manufacturer's instructions, overnight at 4° C. The samples were eluted from the column using SDS buffer (2% SDS, 100 mM Tris-HCl pH 7.2, 10 mM DTT). After immunoprecipitation, the protein eluates were precipitated overnight with ice-cold acetone (1:4 v/v) and subjected to sample preparation for proteomics according to previously published procedures (45).

Mass-spectrometry and data analysis-Peptides derived from tryptic digestion (~1 µg) were separated on a reverse phase PicoFrit column (75 um ID, 8 Um tip, 250 mm bed packed with Reprosil-PUR C18-AQ, 1.9 µm particle size, 120 Å pore size, New Objective, Inc., Woburn, MA, USA, cat. PF7508-250H363), using an EASY-nLC™ 1200 System (Thermo Fisher Scientific, Waltham, MA, USA). Total run time for each sample was 120 min, peptides were separated using a 100 min gradient (4–40% acetonitrile +0.1% formic acid at 300 nL/min). Eluting peptides were measured on-line with a Q Exactive HF benchtop mass spectrometer (Thermo Fisher Scientific) operating in data-dependent acquisition mode (Top20). Peptides were ionized at a potential of +2 KV, intact peptide ions were detected at a resolution of 120,000 (at m/z 200) and fragment ions at a resolution of 15,000 (at m/z 200); AGC Target settings for MS were $3{\cdot}10^6$ charges and for MS/MS $1{\cdot}10^5$ charges. Peptides were selected for Higher-energy C-trap dissociation (HCD) fragmentation with a quadrupole isolation window of 1.4 Th, peptides were fragmented at a normalized collision energy of 30. The intensity threshold was set at $2{\cdot}10^4$ and Dynamic exclusion at 30 s. Raw files from MS analysis were processed using the MaxQuant software version 1.6.10.43 22 (Martinsried, Germany) [15]. The spectra were searched against a Uniprot human database (release 2020_2, 20,375 sequences, including isoforms). Precursor and fragment mass tolerance were set to 7 and 20 ppm., respectively, while the minimum length of the peptide was set to 7. False discovery rate (FDR) was set to 1% both at the peptide and protein level. Enzyme for *in silico* digestion were set to trypsin and lysine C, and up to two missed cleavages were allowed. Cysteine carbamidomethylation (Cys, +57.021464 Da) was set as a fixed modification, whereas N-acetylation of proteins (N-terminal, +42.010565 Da) and oxidized methionine (Met, +15.994915 Da) were included as variable modifications.

Proteins identified and quantified via LC-MS/MS were analysed using different bioinformatics tools to distinguish interactors from false positives and obtain a list of candidates constituting the core local network of AGT proteoforms. Label-free quantification of proteins were performed using spectral counts, while the Significance Analysis of INTeractome (SAINT) approach was used for scoring the significance of the interactions (46-48). This method estimates the distribution of protein abundances under true and false interaction hypotheses and computes the probability of true interaction, taking into account the information from negative controls included in the experimental setup. Our negative controls were represented

bioRxiv preprint doi: https://doi.org/10.1101/2021.05.24.445519; this version posted May 25, 2021. The copyright holder for this preprint (which was not certified by peer review) is the author/funder, who has granted bioRxiv a license to display the preprint in perpetuity. It is made available under aCC-BY-NC-ND 4.0 International license.

by wild-type HEK293 cells not expressing AGT (Ctrl, n=3) and HEK293 expressing the AGT-Ma or AGT-Mi isoforms subjected to the co-IP without the AGT antibody. Scored interaction by the SAINT algorithm were filtered using a fold change vs controls > 2 and a SAINT score (SP score)>0.7.

Network visualization was performed using the Cytoscape software as previously reported (49). The mass spectrometry proteomics data have been deposited to the ProteomeXchange Consortium via the PRIDE (50) partner repository with the dataset identifier PXD025661.

Author contributions

B.C., G.G., P.L. and M.D. conceived the project. M.D., G.G., S.P., D.C., S.G., G. U. performed experiments. B.C., P.L., G.G., M.D., D.C., C.C. analysed experimental data. B.C., P.L. and G.G. wrote the manuscript with the input from all the authors.

Acknowledgments

The authors would like to thank the Scientific Computing and Data Analysis section of Research Support Division at OIST for the support provided for the molecular dynamics simulations. We thank Gioena Pampalone for technical support and useful discussion. The authors would also like to thank Prof. Stefano Gianni and Dr. Ben Clifton for critical reading and feedback on the manuscript.

Funding

Sapienza University of Rome n.RP11916B407928AA to G.G.; Oxalosis and Hyperoxaluria Foundation to B.C.; Financial support by the Okinawa Institute of Science and Technology to P.L. is gratefully acknowledged; M.D. thanks Japan Society for the Promotion of Science (JSPS). Fellowship number: P19764

Conflict of interest

The authors declare no conflict of interest

References

1 Gibson, G. and Dworkin, I. (2004) Uncovering cryptic genetic variation. *Nature reviews. Genetics*, **5**, 681-690.

2 Paaby, A.B. and Rockman, M.V. (2014) Cryptic genetic variation: evolution's hidden substrate. *Nature reviews. Genetics*, **15**, 247-258.

3 Zheng, J., Payne, J.L. and Wagner, A. (2019) Cryptic genetic variation accelerates evolution by opening access to diverse adaptive peaks. *Science*, **365**, 347-353.

4 Gianni, S., Freiberger, M.I., Jemth, P., Ferreiro, D.U., Wolynes, P.G. and Fuxreiter, M. (2021) Fuzziness and Frustration in the Energy Landscape of Protein Folding, Function, and Assembly. *Acc Chem Res*, **54**, 1251-1259.

bioRxiv preprint doi: https://doi.org/10.1101/2021.05.24.445519; this version posted May 25, 2021. The copyright holder for this preprint (which was not certified by peer review) is the author/funder, who has granted bioRxiv a license to display the preprint in perpetuity. It is made available under aCC-BY-NC-ND 4.0 International license.

5 Babu, M.M. (2016) The contribution of intrinsically disordered regions to protein function, cellular complexity, and human disease. *Biochemical Society transactions*, **44**, 1185-1200.
6 Liu, Z. and Huang, Y. (2014) Advantages of proteins being disordered. *Protein science : a publication of the Protein Society*, **23**, 539-550.
7 Cellini, B., Bertoldi, M., Montioli, R., Paiardini, A. and Borri Voltattorni, C. (2007) Human wild-type alanine:glyoxylate aminotransferase and its naturally occurring G82E variant: functional properties and physiological implications. *The Biochemical journal*, **408**, 39-50.
8 Oppici, E., Montioli, R. and Cellini, B. (2015) Liver peroxisomal alanine:glyoxylate aminotransferase and the effects of mutations associated with Primary Hyperoxaluria Type I: An overview. *Biochimica et biophysica acta*, **1854**, 1212-1219.
9 Lorenzo, V., Torres, A. and Salido, E. (2014) Primary hyperoxaluria. *Nefrologia : publicacion oficial de la Sociedad Espanola Nefrologia*, **34**, 398-412.
10 Purdue, P.E., Takada, Y. and Danpure, C.J. (1990) Identification of mutations associated with peroxisome-to-mitochondrion mistargeting of alanine/glyoxylate aminotransferase in primary hyperoxaluria type 1. *The Journal of cell biology*, **111**, 2341-2351.
11 Lumb, M.J. and Danpure, C.J. (2000) Functional synergism between the most common polymorphism in human alanine:glyoxylate aminotransferase and four of the most common disease-causing mutations. *The Journal of biological chemistry*, **275**, 36415-36422.
12 Danpure, C.J. (2006) Primary hyperoxaluria type 1: AGT mistargeting highlights the fundamental differences between the peroxisomal and mitochondrial protein import pathways. *Biochimica et biophysica acta*, **1763**, 1776-1784.
13 Mesa-Torres, N., Salido, E. and Pey, A.L. (2014) The lower limits for protein stability and foldability in primary hyperoxaluria type I. *Biochimica et biophysica acta*, **1844**, 2355-2365.
14 Cellini, B., Montioli, R. and Voltattorni, C.B. (2011) Human liver peroxisomal alanine:glyoxylate aminotransferase: characterization of the two allelic forms and their pathogenic variants. *Biochimica et biophysica acta*, **1814**, 1577-1584.
15 Hopper, E.D., Pittman, A.M., Fitzgerald, M.C. and Tucker, C.L. (2008) In vivo and in vitro examination of stability of primary hyperoxaluria-associated human alanine:glyoxylate aminotransferase. *The Journal of biological chemistry*, **283**, 30493-30502.
16 Mesa-Torres, N., Fabelo-Rosa, I., Riverol, D., Yunta, C., Albert, A., Salido, E. and Pey, A.L. (2013) The role of protein denaturation energetics and molecular chaperones in the aggregation and mistargeting of mutants causing primary hyperoxaluria type I. *PloS one*, **8**, e71963.
17 Cellini, B., Lorenzetto, A., Montioli, R., Oppici, E. and Voltattorni, C.B. (2010) Human liver peroxisomal alanine:glyoxylate aminotransferase: Different stability under chemical stress of the major allele, the minor allele, and its pathogenic G170R variant. *Biochimie*, **92**, 1801-1811.
18 Montioli, R., Fargue, S., Lewin, J., Zamparelli, C., Danpure, C.J., Borri Voltattorni, C. and Cellini, B. (2012) The N-terminal extension is essential for the formation of the active dimeric structure of liver peroxisomal alanine:glyoxylate aminotransferase. *The international journal of biochemistry & cell biology*, **44**, 536-546.
19 Dindo, M., Mandrile, G., Conter, C., Montone, R., Giachino, D., Pelle, A., Costantini, C. and Cellini, B. (2020) The ILE56 mutation on different genetic backgrounds of alanine:glyoxylate aminotransferase: Clinical features and biochemical characterization. *Molecular genetics and metabolism*, **131**, 171-180.
20 Cellini, B., Montioli, R., Paiardini, A., Lorenzetto, A., Maset, F., Bellini, T., Oppici, E. and Voltattorni, C.B. (2010) Molecular defects of the glycine 41 variants of alanine glyoxylate aminotransferase associated with primary hyperoxaluria type I. *Proceedings of the National Academy of Sciences of the United States of America*, **107**, 2896-2901.
21 van der Lee, R., Buljan, M., Lang, B., Weatheritt, R.J., Daughdrill, G.W., Dunker, A.K., Fuxreiter, M., Gough, J., Gsponer, J., Jones, D.T. *et al.* (2014) Classification of intrinsically disordered regions and proteins. *Chem Rev*, **114**, 6589-6631.

bioRxiv preprint doi: https://doi.org/10.1101/2021.05.24.445519; this version posted May 25, 2021. The copyright holder for this preprint (which was not certified by peer review) is the author/funder, who has granted bioRxiv a license to display the preprint in perpetuity. It is made available under aCC-BY-NC-ND 4.0 International license.

22 Dindo, M., Conter, C. and Cellini, B. (2017) Electrostatic interactions drive native-like aggregation of human alanine:glyoxylate aminostransferase. *The FEBS journal*, **284**, 3739-3764.
23 Parra, R.G., Schafer, N.P., Radusky, L.G., Tsai, M.Y., Guzovsky, A.B., Wolynes, P.G. and Ferreiro, D.U. (2016) Protein Frustratometer 2: a tool to localize energetic frustration in protein molecules, now with electrostatics. *Nucleic acids research*, **44**, W356-360.
24 Strodel, B., Whittleston, C.S. and Wales, D.J. (2007) Thermodynamics and kinetics of aggregation for the GNNQQNY peptide. *J Am Chem Soc*, **129**, 16005-16014.
25 Fernandez-Higuero, J.A., Betancor-Fernandez, I., Mesa-Torres, N., Muga, A., Salido, E. and Pey, A.L. (2019) Structural and functional insights on the roles of molecular chaperones in the mistargeting and aggregation phenotypes associated with primary hyperoxaluria type I. *Adv Protein Chem Struct Biol*, **114**, 119-152.
26 Forcelloni, S. and Giansanti, A. (2020) Mutations in disordered proteins as early indicators of nucleic acid changes triggering speciation. *Scientific reports*, **10**, 4467.
27 Birdsey, G.M., Lewin, J., Cunningham, A.A., Bruford, M.W. and Danpure, C.J. (2004) Differential enzyme targeting as an evolutionary adaptation to herbivory in carnivora. *Molecular biology and evolution*, **21**, 632-646.
28 Schuch, J.B., Paixao-Cortes, V.R., Friedrich, D.C. and Tovo-Rodrigues, L. (2016) The contribution of protein intrinsic disorder to understand the role of genetic variants uncovered by autism spectrum disorders exome studies. *Am J Med Genet B Neuropsychiatr Genet*, **171B**, 479-491.
29 Vacic, V. and Iakoucheva, L.M. (2012) Disease mutations in disordered regions--exception to the rule? *Molecular bioSystems*, **8**, 27-32.
30 Qiu, J., Nechaev, D. and Rost, B. (2020) Protein-protein and protein-nucleic acid binding residues important for common and rare sequence variants in human. *BMC Bioinformatics*, **21**, 452.
31 Waterhouse, A., Bertoni, M., Bienert, S., Studer, G., Tauriello, G., Gumienny, R., Heer, F.T., de Beer, T.A.P., Rempfer, C., Bordoli, L. *et al.* (2018) SWISS-MODEL: homology modelling of protein structures and complexes. *Nucleic acids research*, **46**, W296-W303.
32 Rodrigues, J., Teixeira, J.M.C., Trellet, M. and Bonvin, A. (2018) pdb-tools: a swiss army knife for molecular structures. *F1000Res*, **7**, 1961.
33 Gupta, S., Kelow, S., Wang, L., Andrake, M.D., Dunbrack, R.L., Jr. and Kruger, W.D. (2018) Mouse modeling and structural analysis of the p.G307S mutation in human cystathionine beta-synthase (CBS) reveal effects on CBS activity but not stability. *The Journal of biological chemistry*, **293**, 13921-13931.
34 Abraham, M.J., Murtola, T., Schulz, R., Páll, S., Smith, J.C., Hess, B. and Lindahl, E. (2015) GROMACS: High performance molecular simulations through multi-level parallelism from laptops to supercomputers. *SoftwareX*, **1-2**, 19-25.
35 Brooks, B.R., Brooks, C.L., 3rd, Mackerell, A.D., Jr., Nilsson, L., Petrella, R.J., Roux, B., Won, Y., Archontis, G., Bartels, C., Boresch, S. *et al.* (2009) CHARMM: the biomolecular simulation program. *J Comput Chem*, **30**, 1545-1614.
36 Izadi, S., Anandakrishnan, R. and Onufriev, A.V. (2014) Building Water Models: A Different Approach. *J Phys Chem Lett*, **5**, 3863-3871.
37 Bussi, G., Donadio, D. and Parrinello, M. (2007) Canonical sampling through velocity rescaling. *J Chem Phys*, **126**, 014101.
38 Parrinello, M. and Rahman, A. (1981) Polymorphic transitions in single crystals: A new molecular dynamics method. *Journal of Applied Physics*, **52**, 7182-7190.
39 Darden, T., York, D. and Pedersen, L. (1993) Particle mesh Ewald: An N·log(N) method for Ewald sums in large systems. *The Journal of Chemical Physics*, **98**, 10089-10092.
40 Giardina, G., Paiardini, A., Montioli, R., Cellini, B., Voltattorni, C.B. and Cutruzzola, F. (2017) Radiation damage at the active site of human alanine:glyoxylate aminotransferase reveals that the cofactor position is finely tuned during catalysis. *Scientific reports*, **7**, 11704.
41 Papoian, G.A., Ulander, J., Eastwood, M.P., Luthey-Schulten, Z. and Wolynes, P.G. (2004) Water in protein structure prediction. *Proceedings of the National Academy of Sciences of the United States of America*, **101**, 3352-3357.

bioRxiv preprint doi: https://doi.org/10.1101/2021.05.24.445519; this version posted May 25, 2021. The copyright holder for this preprint (which was not certified by peer review) is the author/funder, who has granted bioRxiv a license to display the preprint in perpetuity. It is made available under aCC-BY-NC-ND 4.0 International license.

42 Humphrey, W., Dalke, A. and Schulten, K. (1996) VMD: visual molecular dynamics. *J Mol Graph*, **14**, 33-38, 27-38.
43 Oppici, E., Roncador, A., Montioli, R., Bianconi, S. and Cellini, B. (2013) Gly161 mutations associated with Primary Hyperoxaluria Type I induce the cytosolic aggregation and the intracellular degradation of the apo-form of alanine:glyoxylate aminotransferase. *Biochimica et biophysica acta*, **1832**, 2277-2288.
44 Miyazaki, K. (2011) MEGAWHOP cloning: a method of creating random mutagenesis libraries via megaprimer PCR of whole plasmids. *Methods in enzymology*, **498**, 399-406.
45 Macchioni, L., Chiasserini, D., Mezzasoma, L., Davidescu, M., Orvietani, P.L., Fettucciari, K., Salviati, L., Cellini, B. and Bellezza, I. (2020) Crosstalk between Long-Term Sublethal Oxidative Stress and Detrimental Inflammation as Potential Drivers for Age-Related Retinal Degeneration. *Antioxidants (Basel)*, **10**.
46 Choi, H., Larsen, B., Lin, Z.Y., Breitkreutz, A., Mellacheruvu, D., Fermin, D., Qin, Z.S., Tyers, M., Gingras, A.C. and Nesvizhskii, A.I. (2011) SAINT: probabilistic scoring of affinity purification-mass spectrometry data. *Nat Methods*, **8**, 70-73.
47 Choi, H., Glatter, T., Gstaiger, M. and Nesvizhskii, A.I. (2012) SAINT-MS1: protein-protein interaction scoring using label-free intensity data in affinity purification-mass spectrometry experiments. *J Proteome Res*, **11**, 2619-2624.
48 Guard, S.E., Ebmeier, C.C. and Old, W.M. (2019) Label-Free Immunoprecipitation Mass Spectrometry Workflow for Large-scale Nuclear Interactome Profiling. *J Vis Exp*.
49 Chiasserini, D., van Weering, J.R., Piersma, S.R., Pham, T.V., Malekzadeh, A., Teunissen, C.E., de Wit, H. and Jimenez, C.R. (2014) Proteomic analysis of cerebrospinal fluid extracellular vesicles: a comprehensive dataset. *J Proteomics*, **106**, 191-204.
50 Perez-Riverol, Y., Csordas, A., Bai, J., Bernal-Llinares, M., Hewapathirana, S., Kundu, D.J., Inuganti, A., Griss, J., Mayer, G., Eisenacher, M. *et al.* (2019) The PRIDE database and related tools and resources in 2019: improving support for quantification data. *Nucleic acids research*, **47**, D442-D450.